Numerical Rebuilding of High and Low Enthalpy Hypersonic Flow Test Over a Double Wedge Model

G. Pezzella[⋆†]*, D. de Rosa*[⋆]*, R. S. Donelli*[⋆] *and P. Catalano*[⋆]
[⋆]*CIRA Italian Aerospace Research Centre*
Via Maiorise, Capua, 81043, Italy, g.pezzella@cira.it, d.derosa@cira.it, r.donelli@cira.it and p.catalano@cira.it
[†]Corresponding author

Abstract

In this paper we report and discuss the results of the computational analysis of the flowfield past a double wedge model that has been used in a test campaign performed in the Hypervelocity Expansion Tube (HET) at the University of Illinois. Along with the center of the model, 19 coaxial thermocouple gauges at 16 different streamwise locations are mounted. Therefore, in the present work, numerical-to-experimental comparisons have been carried out in order to address the Shock Wave Boundary Layer Interactions (SWBLI) and resulting heat transfer in hypervelocity double wedge non-equilibrium flow.

1. Introduction

Figure 1 shows the selected geometry for computational analyses. It consists of a double wedge model with $L_1 = 50.8\ mm$, $\theta_1 = 30\ deg$, $L_2 = 25.4\ mm$; $\theta_2 = 55\ deg$, and with width 101.6 *mm* that has been used in a test campaign performed in the Hypervelocity Expansion Tube at the University of Illinois. It was equipped with 19 coaxial thermocouple gauges at 16 different streamwise locations. Therefore, several experimental data are available for numerical-to-experimental comparisons. The scope of the present work is to address the Shock Wave Boundary Layer Interactions and resulting heat transfer.

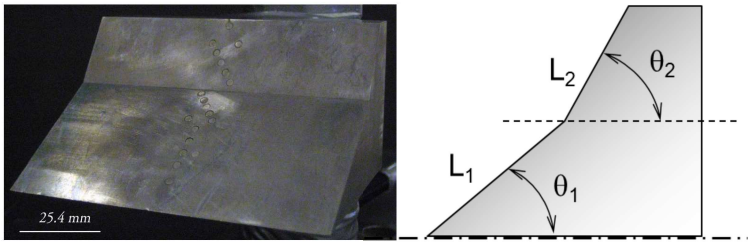

Figure 1: Test bed configuration with quotes

One of the primary technological challenges to the development of hypersonic capabilities is the management of the substantial thermal loads associated with the aerothermodynamic environment. Conservative approaches to thermal protection system (TPS) increase the vehicle weight at the expense of the performance, even if, aggressive, low-weight designs increase the potential risk for structural failure. At the heart of this problem lies the current inability to accurately predict the complex fluid dynamic, thermodynamic and chemical phenomena which dominate the development of thermal loads on hypersonic systems. Two examples of such critical phenomena are the shock wave/boundary layer interactions and the surface heating due to turbulent flow over both localized disturbances and distributed arbitrary roughness.

SWBLI are commonplace in hypersonic aerodynamics. They occur in the vicinity of deflected control surfaces, fuselage-wing junctures, corner flows in inlets and many other locations. Shock interactions can cause boundary layer separation with concomitant high heat transfer at reattachment which has a significant impact on the design of thermal protection systems.

The principal flowfield phenomena that take place in the flow field structure past a double wedge are summarized in Figure 2.

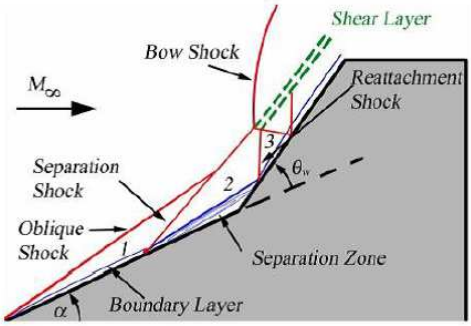

Figure 2: Double wedge model and flow field phenomena

The forward wedge ($\alpha = 30\ deg$) generates an oblique shock wave with inviscid shock angle 39.8 *deg*. The rearward wedge angle ($\alpha + \theta_w = 55\ deg$) exceeds the maximum inviscid flow deflection angle (43.3 *deg*) and hence generates a detached shock wave. The shock wave boundary layer interaction causes separation of the boundary layer on the forward wedge leading to a recirculation region and separation shock wave. The forward wedge oblique shock and separation shock interact to form a triple point above the separation region. A second triple point is formed by the intersection of the separation shock and rearward wedge detached shock resulting in a strong shear layer with subsonic flow above and a shock-expansion train beneath. The reattachment of the boundary layer results in a peak in surface heat transfer. Accurate prediction of shock interactions is therefore essential for optimal design of hypersonic vehicles.

As part of the effort, the numerical rebuilding of two test experimental campaigns (double wedge in nitrogen and air) was undertaken by CIRA in the framework of the STO AVT 205 panel,[1] namely *Assessment of Predictive Capabilities for Aerodynamic Heating of Hypersonic Systems*.

2. Description of Experiment

In the framework of the STO AVT 205 panel, the experiment of Swantek and Austin[2] was selected for the assessment of computational methods for hypersonic shock wave laminar boundary layer interactions. The model geometry comprises a double wedge ($\theta = 30\ deg$ and $\alpha + \theta_w = 55\ deg$) machined from A2 tool steel. The length of the first face is $L_1 = 50.8\ mm$ and the second is $L_2 = 25.4\ mm$. The width of the model is 101.6 *mm*.

The model was dimensioned according to the criteria summarized in[3] and designed as a one-half scale version. A critical parameter is the ratio of the wedge width b to the boundary layer thickness δ at separation. For the experiments investigated in this work, the ratio was $b/\delta \approx 125$. Side fences were not included in order to avoid obstructing the optical path and modifying the separation region.

The experiments were performed in HET at the University of Illinois, Urbana-Champaign.[4] Tests were performed in air and nitrogen at the freestream conditions indicated in Table 1.

Table 1: Freestream Conditions and experimental setup

Parameter	**M7_2**	**M7_8**
Stagnation enthalpy (MJ/Kg)	2.1	8.0
Mach number	7.11	7.14
Static temperature (K)	191	710
Static pressure (kPa)	0.391	0.780
Velocity (m/s)	1972	3812
Density (kg/m^3)	0.0071	0.0038
Unit Reynolds number ($10^6/m$)	1.10	0.435
Test time (microseconds)	327	242

The freestream parameters between air and nitrogen experience a change of less than 0.5% at the same test condition. The model surface temperature is 298 K during the tests. Instrumentation includes nineteen coaxial thermocouples at sixteen different streamwise locations on the model. Three locations have two spanwise gauges to assess possible three dimensional behavior. The locations of the gauges are listed in Table 2 where s is measured from the leading edge of the forward wedge along the surface. The gauges are clustered in areas of interest such as separation, reattachment and shock impingement as indicated from single frame schlieren images.

Table 2: Coaxial Thermocouple Gauge Locations

	Gauge	s (inch)	z (inch)	s/L	z/W
Fore End	A	0.4	0	0.2	0
	B	0.7	0	0.35	0
	C	0.9	0	0.45	0
	C1	0.9	0.162	0.45	0.0405
	D	1.1	0	0.55	0
	E	1.3	0	0.65	0
	F	1.468	-0.162	0.734	-0.045
	F1	1.468	0.162	0.734	0.0405
	G	1.584	0.081	0.792	0.02025
	H	1.7	0	0.85	0
	I	1.816	-0.081	0.908	-0.02025
	J	1.932	-0.162	0.966	-0.0405
Aft End	K	2.119	0.185	1.0595	0.04625
	L	2.251	0.092	1.1255	0.023
	M	2.383	0	1.1915	0
	N	2.515	-0.092	1.2575	-0.023
	O	2.647	-0.185	1.3235	-0.04625
	O1	2.647	0.185	1.3235	0.04625
	P	2.897	0	1.4485	0

The experimental heat transfer data are presented in Figure 3 for the test case having a stagnation enthalpy of 8.0 MJ/kg either in air and in nitrogen.

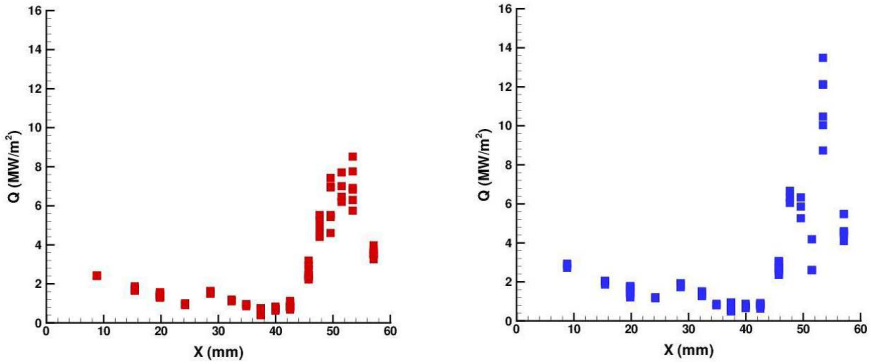

Figure 3: Heat flux versus x for 8.0 MJ/kg in air (left) and N_2 (right)

3. CFD Analysis

The governing equations are the steady Reynolds-averaged compressible Navier-Stokes (RANS) equations. A five species thermochemistry model (N_2, N, O_2, O, NO) is used for air and a two species model (N_2, N) for nitrogen with separate translational-rotational and vibrational temperatures. Ionization phenomenon has been discharged due to rather low flow energy. Three dissociation reactions and two exchange reactions can be considered as reaction mechanism. A reacting partner (i.e., third body) that can be any of the reacting species, is also included. Therefore, the reaction mechanism for air results in a system of 17 chemical reactions, 17 forward and backward reactions rate coefficient, respectively. Chemical kinetics is modeled using an Arrhenius form with Park rates.[5]

A separate vibrational energy equation is used for the mixture vibrational energy with the Landau-Teller[6] model for vibrational-translational energy relaxation and inter-species relaxation rates.[7] Both non-catalytic and fully catalytic surface boundaries were considered for air, and non-catalytic boundary for nitrogen. Viscosity coefficients were calculated from Wilke's semi-empirical rule. Finally, turbulence has been taken into account with the $k-\omega$ SST model.

3.1 Computational Grids

Structure multiblock grids of 433X707 points (i.e., about 0.30 M cells) were considered to solve for complex flow structure of SWBLI. Both computational grids (for air and nitrogen) have been tailored for the experimental test cases setup. A great deal of care was taken in multiblock grid development. In fact, the distribution of grid points has been dictated by the level of resolution desired in various areas of the computational domain such as shock-shock interaction, triple points, shear layer and recirculation region, according to the computational scopes.

To obtain a good quality Navier-Stokes solution, the mesh has been built clustering the points as close as possible to the surface. Moreover, attention was paid to grid density, grid distribution (stretching), and cell Reynolds number at the wall, because heat flux prediction is very sensitive to those mesh features. Grid refinement in strong gradient regions of the flowfield (i.e., shock fitting) was made through a solution adaptive approach and multigrid techniques were used to accelerate convergence. An example of the computational grid is provided in Figure 4.

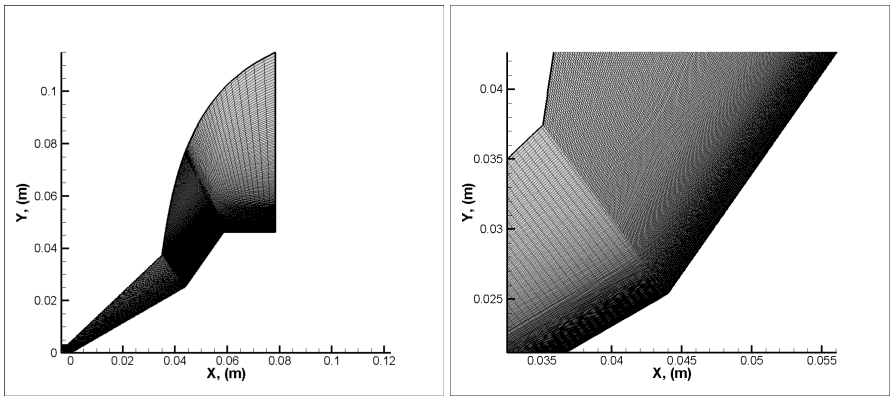

Figure 4: An example of the computational grid

3.2 Test matrix

Computational activities to numerically rebuild the experiments foresaw several test cases. Table 3 shows a summary of the seven CFD computations performed.

Table 3: CFD test matrix

Mach	Flow condition	Wall BC
7.14	LAM	NCW[a]
7.14	X_{tr} = 58%L	NCW
7.14	X_{tr} = 58%L	FCW[b]
7.14	X_{tr} = 82%L	FCW
7.14	X_{tr} = 100%L	NCW
7.30	X_{tr} = 58%L	NCW
7.30	X_{tr} = 65%L	FCW

[a] Non Catalytic Wall
[b] Fully Catalytic Wall

Two Mach numbers and five different flow conditions with and without catalytic effect at wall were considered. The M_∞ = 7.14 simulations are representative of the experimental results. But M_∞ = 7.3 was also considered to assess the Mach number effect. Further, in order to take into account for the effects of the transition of the boundary layer from laminar to turbulent flow, several numerical computations were performed by imposing the transition location. The first CFD computation has been performed in fully laminar flow conditions due to the rather low unit Reynolds number. Once the boundary layer was extracted, a trade-off on the transition location was performed. The transition location has been fixed at x_{tr} = 58% L_1 since it corresponds to the separation point in laminar condition. The other three transition points were located to observe the effect on both heat transfer peak location and intensity; in particular, the x_{tr} = 100% L_1 was set as it corresponds to the hinge line point. Furthermore, the wall catalytic effect was also considered.

3.3 Numerical Results in Air in high enthalpy

The boundary layer on the forward wedge results laminar. In fact, the Reynolds number, based on the length L_1 of the forward wedge and conditions downstream of the forward oblique shock wave, is less than 10^5 for all test cases.

Figure 5 shows the qualitative comparison between experimental (Schlieren image) and steady state numerical data for the fully laminar simulation with NCW boundary conditions. As it can be observed, the contour field differs from the Schlieren since there is no triple point due to a strong shock that originates ahead the recirculation bubble. This numerical result suggested, despite the rather low unit Reynolds number, to investigate also transitional flow conditions.

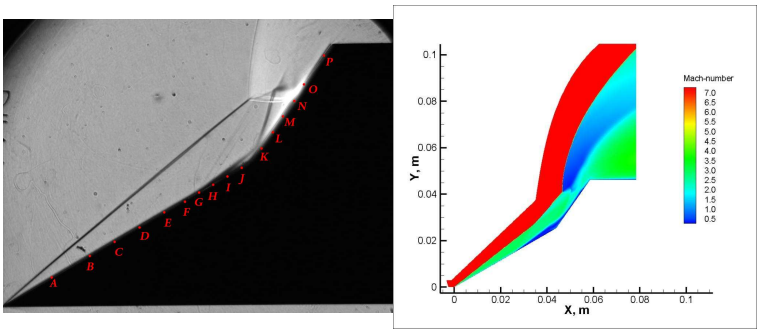

Figure 5: Schlieren image in air (left). Mach number contours for laminar flow (right)

The comparison between flow field contours of the Mach number for the test cases in fully laminar and transitional (x_{tr} = 58% L_1) flow conditions at NCW is shown in Figure 6.

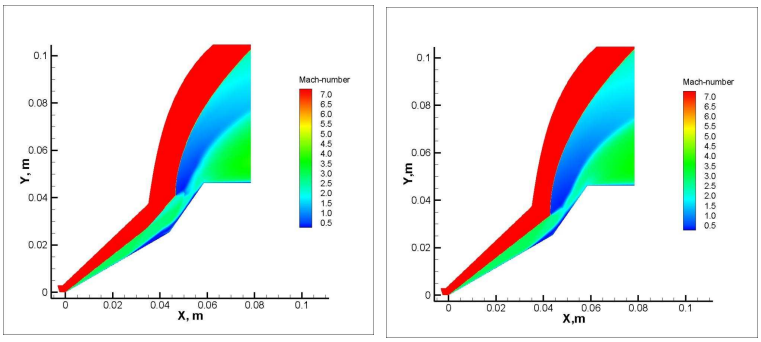

Figure 6: Mach number contours for laminar (left) and transitional flow (right)

The numerical flow field, in the case of transitional simulation, presents the same structure as pointed out by the experimental test case. Indeed, Figure 7 shows the Mach isolines and it is possible to recognize all the features of the flow field structure expected in this case, according to Figure 2.

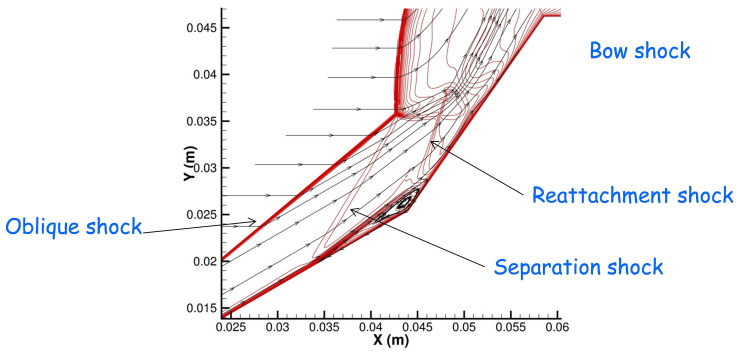

Figure 7: Mach isolines with streamtraces for transitional flow (x_{tr} = 58% L_1) with NCW

As far as transitional abscissa is concerned, it is worth noting that empirical criteria, such as Anderson, Reda et al.[8,9] were implemented to locate transition point. Nevertheless, none of these criteria provided a location for transition as the unit Re number is rather low.[2] The laminar feature of the flow is also highlighted by the shape factor provided in Figure 8. The shape factor is constant and close to the laminar value of the flat plate[10] up to about 0.0027 *m*, which corresponds to the beginning of the separation bubble region.

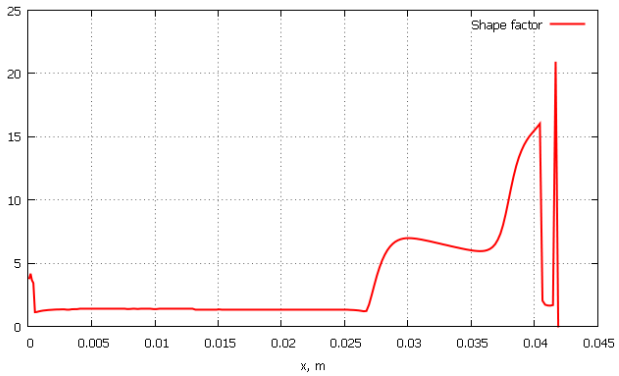

Figure 8: Shape factor for fully laminar simulation with NCW

On the base of this analysis, the separation point observed in fully laminar analysis was set as transition point for laminar-to-turbulent simulations.

The results of heat flux distribution are presented in Figure 9 (left) in the case of non-catalytic wall and of laminar flow. The computed heat transfer is within the experimental uncertainty upstream of the computed separation point at $x = 27\ mm$. According to above discussion, the computed peak heat transfer in the fully laminar flow conditions differs significantly from the experimental data, apart from the laminar region on the first ramp (approx. $x < 0.03\ m$). The computed peak heat flux is less than half the experimental one and its location is further downstream of the experimental peak. On the contrary, results of two separate computations assuming transition of the boundary layer from laminar to turbulent at $x = 29.5\ mm$ ($58\%L_1$) are presented in Figure 9 (right) for both non-catalytic wall and fully catalytic wall .

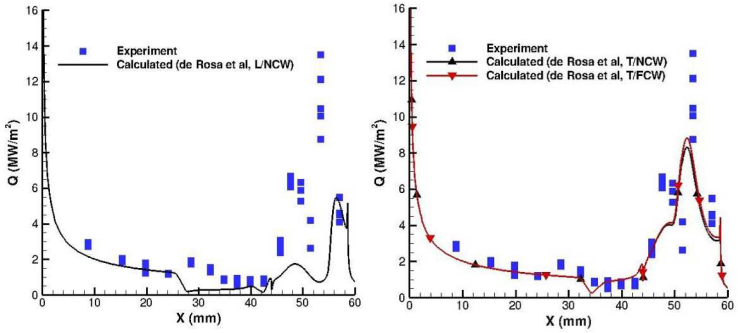

Figure 9: Q vs x. Laminar, NCW (left). Transitional, NCW and FCW (right)

The computed separation point is further downstream ($x \approx 0.034\ m$) as expected due to the increased mixing associated with transition of the boundary layer from laminar to turbulent. The numerical peak heat transfer location compares rather well with the experimental peak, but the numerical simulation under-predicts the peak value by 35% (see Figure 9, right) with respect to the experimental one.

In Figure 10 the effect of the transition location is shown for the test case at $M_\infty = 7.14$. In the laminar region, the match between experimental and numerical results is quite good for every simulation, as expected. Differences arise in the region downstream the transition point (or separation point for fully laminar simulation). The first difference concerns the recirculation zone, whose length depends on the transition location. The widest bubble is obtained for fully laminar condition; while the smallest one refers to the simulation with $x_{tr} = 58\%\ L_1$. The computed separation point is downstream due to the higher energy of the turbulent boundary layer. Anyway, the $x_{tr} = 100\%\ L_1$ determines a rather wider recirculation region, as transition is located inside the bubble. This means that the effect of turbulent boundary layer is less significant. The different bubbles' length affects both heat flux peak and location. For both transition points the computed heat flux peak under-predicts the experimental value by about 43%.

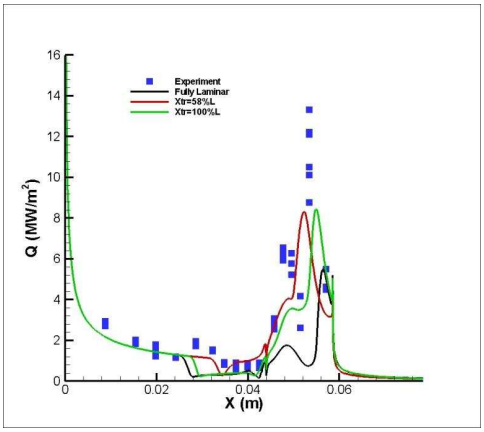

Figure 10: Q vs x. Fully Laminar vs. $x_{tr} = 58\%\ L_1$ and $x_{tr} = 100\%\ L_1$ at NCW

Moreover, the wider the bubble the more downstream results the peak location. This evidence is confirmed also by results provided in Figure 11, where heat flux curves are compared for $x_{tr} = 58\%\ L_1$ and $82\%\ L_1$.

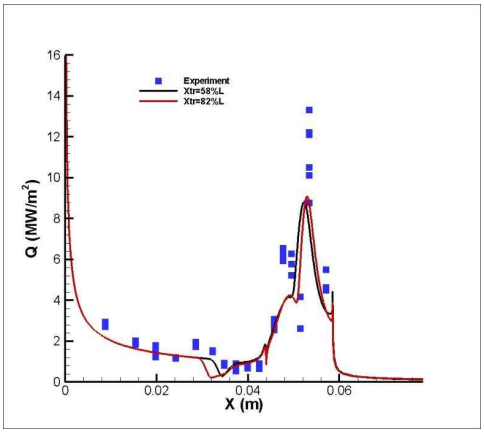

Figure 11: Q vs x. Effect of Transition location at $M_\infty = 7.14$ and NCW

In particular, at $x_{tr} = 58\%\ L_1$ the peak location is just before the position highlighted by experimental data; while numerical result for $x_{tr} = 82\%\ L_1$ is quite close to the experimental one.

As far as Mach number effect is concerned, Figure 12 provides the heat flux comparison for $x_{tr} = 58\%\ L_1$ at $M_\infty = 7.14$ and 7.3.

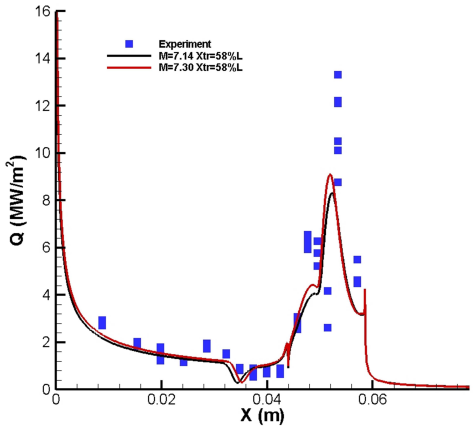

Figure 12: Q vs x. Effect of Transition location at $M_\infty = 7.14$ and $M_\infty = 7.3$ at NCW

As one can see, the values reached in the laminar region are higher for $M_\infty = 7.3$, as expected. Even though transition location is the same, the bubble length is wider for $M_\infty = 7.14$. This effect is due to the lesser energy associated to the boundary layer for this flow condition. As a result, peak location is different, according to above suggestions. Moreover, numerical results at $M_\infty = 7.3$ envisage higher heat flux values but the peak is still under-predicted (by about 35%).

Eventually, Figure 13 shows results for $M_\infty = 7.3$ with $x_{tr} = 58\%\ L_1$ (NCW) and $65\%\ L_1$ (FCW). The higher peak heating is obtained in the case of FCW boundary condition. This simulation, however, still under-predicts the peak experimental value by about 30%.

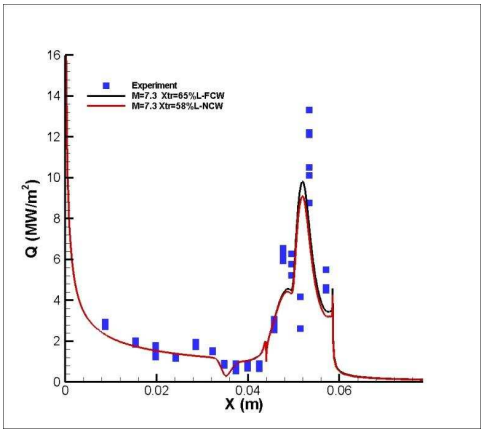

Figure 13: Q vs x. $M_\infty = 7.3$, $x_{tr} = 58\%\ L_1$ and $65\%\ L_1$, NCW and FCW

3.4 Numerical Results for Nitrogen in high enthalpy

The results for Nitrogen test case are presented in Figure 14 assuming transition from laminar-to-turbulent boundary layer fixed at $x = 0.0295\ mm$. Good agreement with experiment is observed over the entire length of the double wedge. The main difference with reference to simulation in air is that, for this analysis, N_2 is starting to dissociate. So, compared to simulations with reacting air mixture, in this case real gas effects appear to be less significant. Thus, the computational complexity is less demanding, leading to better numerical and experimental results comparison.

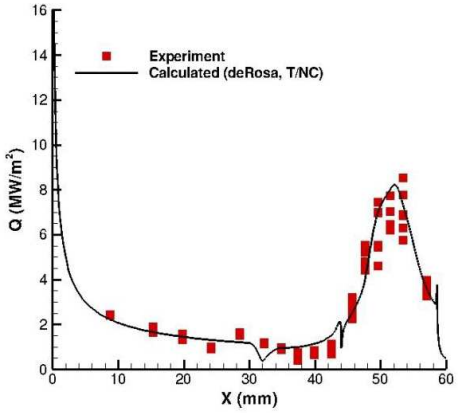

Figure 14: Q vs x. $M_\infty = 7.14$, $x_{tr} = 58\%\ L_1$, NCW

3.5 Numerical Results for Air in low enthalpy

As far as experimental data were available also for the low enthalpy test conditions, the numerical rebuilding was carried out also for this case. In particular, the selected test case is relative to the air mixture. Numerical CFD computations were performed with fully laminar flow and Non Catalytic Wall, being a preliminary attempt to simulate the flowfield

in this condition. Computations are still on-going, anyway, here we report a first comparison with the experimental data in terms of heat flux. Figure 15 shows such comparison and, as it can be seen, a rather well match is found between numerical and experimental data. As shown, numerical results follow the shape of the experimental data quite well, but the maximum heat flux is over-predicted by about 30%.

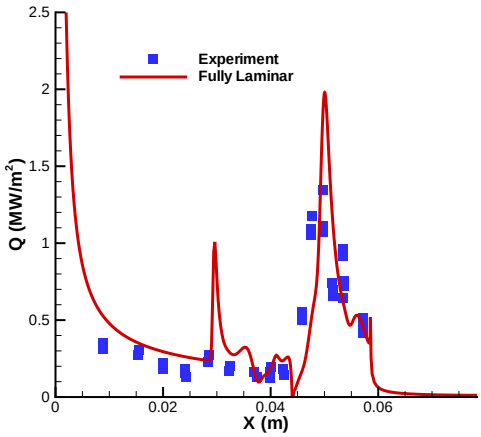

Figure 15: Q vs x. Fully Laminar, NCW, low enthalpy

4. Conclusion

Numerical flow simulations have been performed for both low and high enthalpy conditions. In the case of high enthalpy test the flow seems to be laminar on the first wedge till the separation bubble. Numerical results for transitional flow with $x_{tr} = 58\% L_1$ show the best agreement with experimental data. The numerical and experimental heat flux peak locations compare quite well, while the peak values differ. In particular, numerical results under-predict the maximum heat flux value, at least in the simulations concerning the air mixture. Simulations at $M = 7.3$ were performed to study the effects of increased Mach number and present an increment in heat flux peak but still lower than the experimental data. For the Nitrogen flow, in high enthalpy the comparison between experimental and numerical data is satisfactory.

Preliminary analyses for the air mixture in low enthalpy environment were started and still on-going. Computational fluid dynamics analyses were performed with fully laminar flow and Non Catalytic Wall, being a preliminary attempt to simulate the flowfield in this condition. Numerical results follow the shape of the experimental data quite well, but the maximum heat flux is over-predicted by about 30%. Further analyses are foreseen by considering also Nitrogen and the effect of flow transition/separation.

Acknowledgments

Authors wish to express their gratitude to Prof. Doyle D. Knight of the School of Engineering of Rutgers - The State University of New Jersey, for his support to get ready this paper in the framework of the STO AVT 205 panel.

References

[1] “Assessment of Predictive Capabilities for Aerodynamic Heating of Hypersonic Systems”, RTO Technical Report - STO AVT 205

[2] Swantek, A.B., Austin, J. M., “Heat Transfer on a Double Wedge Geometry in Hypervelocity Air and Nitrogen Flows”, 50th *AIAA Aerospace Sciences Meeting including the New Horizons Forum and Aerospace Exposition*. 09-12 Jan 2012, Nashville, Tennessee. AIAA 2012-0284

[3] Davis, J. and Sturtevant, B., “Separation Length in High-Enthalpy Shock/Boundary Layer Interaction”, *Physics of Fluids*, Vol. 12, No. 10, 2000, pages 2661–2687

[4] Dufrene, A., Sharma, M. and Austin, J., “Design and Characterization of a Hypervelocity Expansion Tube Facility”, *Journal of Propulsion and Power*, Vol. 23, No. 6, 2007, pages 1185–1193

[5] Park, C. *Nonequilibrium Hypersonic Aerothermodynamics*, John Wiley & Sons, New York, NY, 1990

[6] Vincenti, W. and Kruger, C., *Introduction to Physical Gas Dynamics*, Krieger Publishing Company, Malabar, FL, 1965

[7] Millikan, R. and White, D., “Systematics of Vibrational Relaxation”, *Journal of Chemical Physics*, Vol. 39, 1963, pages 3209–3213

[8] Anderson, J. D., “Hypersonic and high-temperature gas dynamics”, AIAA Education Series, AIAA, 2006

[9] Anderson, A. D., “Passive Nosetip Technology (PANT) Program. Volume III. Surface Roughness Effects, Part 3. Boundary Layer Transition Correlation and Analysis”, Interim Report SAMSO-TR-74-86, Vol. III, Pt. I, U.S. Air Force, Jan. 1974

[10] Schlichting, H., *Boundary-Layer Theory*, 8^{th} ed., Springer, 2000